THE JOURNAL OF PHYSICAL CHEMISTRY C

Article

Cite This: J. Phys. Chem. C XXXX, XXX, XXX–XXX

pubs.acs.org/JPCC

Toward Controlled Morphology of FeCu Nanoparticles: Cu Concentration and Size Effects

Javier Rojas-Nunez,[†,∥] Rafael I. Gonzalez,[‡,∥] Eduardo M. Bringa,[§] Sebastian Allende,[†,∥] Pamela Sepúlveda,[∥,⊥] Nicolás Arancibia-Miranda,[∥,⊥] and Samuel E. Baltazar*[,†,∥]

[†]Departamento de Física, Universidad de Santiago de Chile, Av. Ecuador 3493, Santiago 9170124, Chile

[‡]Centro de Nanotecnología Aplicada, Facultad de Ciencias, Universidad Mayor, Santiago 8580745, Chile

[§]CONICET & Facultad de Ciencias Exactas y Naturales, Universidad Nacional de Cuyo, Mendoza, Argentina

[∥]Centro para el desarrollo de Nanociencia y Nanotecnología CEDENNA, Santiago 9170022 Chile

[⊥]Facultad de Química y Biología, Universidad de Santiago de Chile, Casilla 40, Santiago C.P. 33, Chile

Supporting Information

ABSTRACT: Bimetallic nanoparticles (NPs) can be tailored by varying the concentration of their constituent elements, resulting in novel structures and/or configurations, leading to interesting electronic, mechanical, and chemical properties. In this paper, by means of molecular dynamics calculations, we study the morphology of bimetallic FeCu NPs as a function of the Cu concentration. Our results evidence a core−shell (CS) structure for low Cu concentrations and a Janus (JN)-like morphology for high Cu content. Structural and energy characterizations were performed to determine the atomic-scale behavior of the NPs. Using a continuous model to describe immiscible components, we obtain a stability transition curve between CS and JN-like structures for several NP sizes and concentrations. Results from both methods are compared with experimental data obtained for NPs with low and high Cu content, evidencing a good agreement among the three approaches.

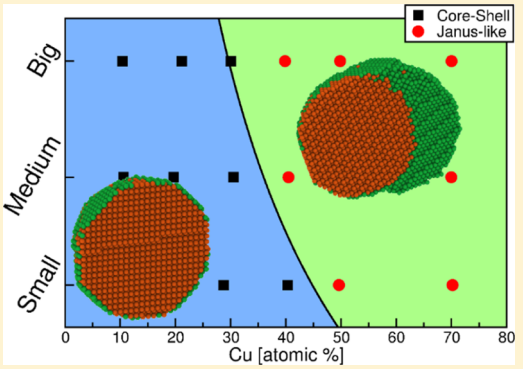

1. INTRODUCTION

Bimetallic nanoparticles (NPs) are novel materials of great scientific and technological relevance because of their unique properties related to the synergistic behavior of both metals. Studies of their properties have been extensively reported, both experimental and theoretically,[1,2] because their mechanical, magnetic, and chemical properties are modified, with respect to the monometallic NPs. Their applications can be addressed in groundwater and soil remediation,[3,4] catalysis,[5] electrochemistry,[6] biomedicine,[7] and optics,[1] among others. In particular, the study of transition-metal clusters and metallic alloys has also been developed both theoretically and experimentally, with great interest in the applications for the removal of contaminants.[4,8,9] One of these transition metals is Fe, which is extensively used in catalysis processes and removal of contaminants.[10] The interaction between a corrosive metal such as Fe and a noble metal such as Au, Cu, Ag, or Pd, establishes a synergic system,[3,11−13] for example, in the FeCu system, where Fe contributes as a precursor material with a negative redox potential, while Cu contributes as a catalyst with a positive redox potential.

In this context, there are some studies focused on the application of FeCu bimetallic NPs into the removal process of heavy metals such as Cr and metalloids.[9] Here, Cu plays an important role to delay the oxidation processes of the corrosive metals,[13] and therefore, it is important to know how the inclusion of Cu modifies the structural configuration. Additionally, this mixing can be accompanied with a modification of their catalytic properties.[5,14] The combination of Fe and Cu elements has been experimentally studied as an alloyed system.[15] In particular, there are some reports arguing the immiscibility of Fe and Cu in bulk,[16] while melting point transitions in small atomic FeCu clusters have also been theoretically investigated.[17] In a similar way, the melting of Janus (JN) and core−shell (CS) Ni−Co NPs was recently explored, for radii smaller than 1.6 nm.[18] Besides this, Erhart et al. studied theoretically the precipitation of Cu in an Fe matrix to find a polymorphic phase diagram of Cu clusters.[19] Although these studies are oriented to consider the mixing effect in other bimetallic systems,[20] insufficient research has been done to evaluate the morphology at different Cu concentrations and particle sizes at the nanoscale that can be related to experimental results.

In this work, we study the stability of FeCu NPs as a function of the Cu concentration and diameter size, with an optimization process, leading to stable atomic configurations. By means of

Received: November 23, 2017
Revised: February 17, 2018
Published: March 26, 2018

DOI: 10.1021/acs.jpcc.7b11556
J. Phys. Chem. C XXXX, XXX, XXX−XXX

structural characterization, we study the preferred morphologies at different Fe and Cu concentrations and the appearance of possible defects in the stabilized NPs, as well as the energy contributions to the bimetallic systems. Additionally, a continuous model is proposed to explain the effect of different energy contributions to the resulting morphology. These approaches can help to the design of novel materials with tailored properties for technological applications.[21] Finally, some experimental evidence on the morphology of bimetallic NPs is shown to compare to our results.

2. METHODOLOGY

We study in this work FeCu bimetallic nanoclusters with different sizes and concentrations. The sizes are separated in three categories, depending on the number of Fe atoms contained in each particle. The first category contains 6183 Fe atoms (~5 nm diameter) and is called the "small" category. The second one contains 15 473 Fe atoms (~7 nm diameter), receiving the name "medium". The last one contains 32 743 Fe atoms (~9 nm diameter) and is named the "big" category. For these sizes, concentrations of around 10, 20, 30, 40, 50, and 70% were considered by adding different amounts of Cu atoms to the Fe NP. For example, at small sizes, we used 791, 1710, 2490, 4178, 6092, and 14 579 Cu atoms, respectively, while at medium sizes we considered 1832, 3788, 6794, 10 526, 15 448, and 36 096 Cu atoms, and finally for big sizes, we used 3780, 8780, 14 054, 21 968, 32 530, and 76 542 Cu atoms, respectively.

To calculate the total energy and simulate the structural optimization of these bimetallic clusters, we have performed classical molecular dynamics simulations because of their good agreement with experimental observations and because they provide a good representation of crystalline phases and cluster structures.[17] Calculations were performed using the LAMMPS software,[22] with analysis carried out using OVITO.[23]

2.1. Computational Methods. The classical molecular simulations were performed under the NVT canonical ensemble, using the Nosé–Hoover thermostat to control the temperature of the system. The interactions between the Fe and Cu atoms were modeled using an embedded atom method potential,[24] whose parameters are taken from the work of Bonny et al.[25] This potential shows a good description of elastic properties, diffusion dynamics, and thermal transport coefficients.[26]

To obtain stable atomic configurations, a structural optimization routine consisting of several cycles of thermal annealing and minimization was adopted. The annealing processes are made of a 5 ps heating ramp going from 20 K to an equilibrium temperature (T_e), a thermal equilibration run during 3 ns at T_e, and finally a 5 ps cooling ramp from T_e to 0.1 K. The energy minimization process, applied after the annealing routine, involves a conjugate gradient and FIRE[27] minimization algorithms, which were used iteratively in succession until a relative energy difference threshold of 0.0001% is reached for the system energy. At the end of each cycle, the structure and its energy are stored for further analysis.

These cycles are repeated until the deviation of the last 10 configuration energies gets below 0.5% of the mean value of these energies. Then, final cooling is performed, starting after the thermal equilibration of the cycle with the lowest energy configuration. This final cooling process is performed slower than the previous ones, at a rate of 0.25 K/ps, and it is followed by a thermal equilibration run at 300 K during 3.1 ns and ending with the same minimization process previously applied to obtain a relaxed final structure.

For our simulations, T_e is selected to be lower than the expected melting temperature for NPs, which is about 10–20% lower than the bulk melting temperature, such as for Ni,[28] Fe,[29,30] and face-centered cubic (fcc) NPs,[31,32] because of the radii considered here. Our annealing temperature is intended to keep the NPs solid at all times by the use of a T_e lower than the lowest expected melting temperature because a T_e above the melting point will produce a quenching effect over NPs after the cooling process, carrying the system away from the global minimum.

2.2. Setting Up Initial Structures. The bimetallic systems involved in these simulations have different mobilities for each element; therefore, a high T_e suitable for Fe will cost a quenching effect on Cu, while a suitable T_e for Cu will be insufficient to move Fe atoms during the simulation time. Because of this, the initial structures are built from previously optimized monoatomic structures of Fe and Cu at T_e of 1300 and 950 K, respectively. The monoatomic optimized clusters were used to build CS and JN as initial structures. These CS and JN structures were chosen as initial structures because of their energetically favorable morphology for the FeCu system (see Figure 1). The CS structures were designed, wrapping an optimized Fe core with an fcc Cu shell, and the JN structures were built, setting a Fe and a Cu optimized cluster next to each other. These initial structures were then optimized with a T_e of 950 K during enough cycles to ensure energy convergence. Finally, the most stable systems at each size and Cu concentration were selected for further analysis.

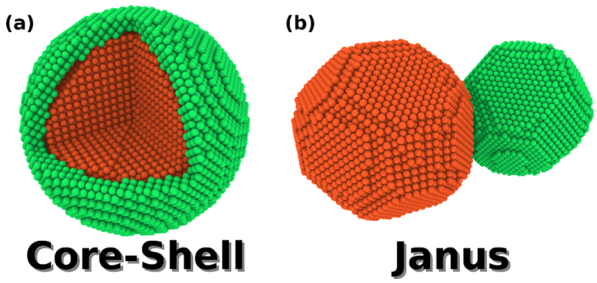

Figure 1. Initial configurations of bimetallic NPs with Fe (orange) and Cu (green): (a) CS structure with a Fe core and Cu shell and (b) JN-like structure.

2.3. Energy Calculation for Initial Structures. The analysis performed in this work requires the calculation of the energy associated with the initial JN and CS structures. This calculation is obtained by means of a short molecular dynamics simulation, which is made of 5 ps of heating from 20 to 300 K, followed by a constant temperature simulation of 0.2 ns and the same energy minimization process applied in the optimization routine. These simulations give us an initial nonoptimized comparison point (E_I^{CS} and E_I^{JN}) for later energy analysis to the different configurations obtained from the optimization routines.

3. RESULTS

To establish the most energetically stable structure for bimetallic NPs, we have to consider different possible atomic arrangements, allowing the exploration of a larger configuration space by means of simulated annealing processes. Additionally, we have evaluated the minimization of alloyed (mixed

DOI: 10.1021/acs.jpcc.7b11556
J. Phys. Chem. C XXXX, XXX, XXX–XXX

interatomic elements) NPs as well as isolated Fe and Cu clusters, being consistently less stable than the two chosen morphologies. Because the Cu concentration has been experimentally associated to different properties of the bimetallic NPs, we have considered the study of $Fe_{1-x}Cu_x$ systems, with x going approximately from 0.1 to 0.7. The NP size effect has also been studied, considering three Fe cores: 5 (small), 7 (medium), and 9 (big) nm of diameter, along with their respective Cu concentrations.

3.1. Relative Energies. From the two different initial structures, we have performed a comparison of the potential energy, at each Cu concentration, between CS and JN structures, after the searching and minimization processes were applied. The energy difference between the most stable configuration obtained E_F and the respective less stable configuration (CS or JN) is shown in Figure 2, as a function of size and Cu content (where 0 and 100% of Cu corresponds to monoatomic systems).

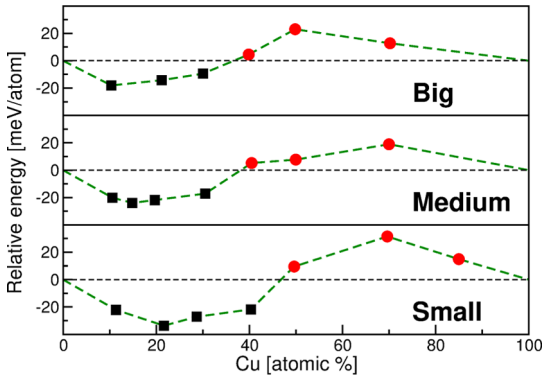

Figure 2. Energy differences between the most stable structures and the least stable structures considered, as a function of the Cu concentration and three different sizes. Negative values correspond to CS structures while positive values are associated to JN-like systems.

The relative energy is then obtained as

$$E_R = \begin{cases} E_F - E_I^{JN}, & \text{if } E_F = E_F^{CS} \\ E_I^{CS} - E_F, & \text{if } E_F = E_F^{JN} \end{cases} \quad (1)$$

where E_I^{JN} and E_I^{CS} are the energies of the initial JN and CS structures. The negative values (black squares) are then associated to a CS-like final structure as the most stable result, while positive values (red circles) represent values where a JN-like final structure was found to be more stable than CS. Here, we can see that at low Cu percentages, CS structures are energetically preferred until a Cu concentration threshold, where JN-like structures become more stable than CS structures.

Additionally, we can see that the mentioned Cu concentration threshold is shifted to the left as the NP size is increased from small to medium (going from 46 to 38% of Cu approximately) and then slightly shifted from medium to big. This result suggests that we can expect both phases as the cluster is enlarged, while a CS structure is preferred as the NP size is diminished.

If we consider the behavior of the energy interactions in FeCu particles (see Table S1 in the Supporting Information), as a function of the Cu percentage, the Fe−Fe contribution to the total energy is nearly the same for a given size. The Cu−Cu contribution becomes more important as the Cu percentage is increased. Finally, the Fe−Cu interaction shows a non-monotonic behavior, starting with a large contribution at low Cu % and then diminishing until it reaches a small energy value of around 30−40%. After this Cu percentage, the energy contribution is slightly increased, and finally, the Fe−Cu interaction drops slowly until a 70% of Cu is reached, a behavior that will be correlated with the morphology.

3.2. Structural Configuration of FeCu NPs. A summary of the structural configurations found for energetically optimized FeCu NPs is shown in Figure 3a, with a cross-sectional view of the atomic structures, as a function of the size and Cu percentage (Figure 3b), where we have identified three characteristic Cu percentages (I: 10%, II: 40%, and III: 70%). At the low Cu percentage (10%), we can see that Fe atoms (brown spheres) are mainly arranged as a compact particle, whereas Cu atoms (green spheres) are distributed around the Fe core. At 70% of Cu, the structure is basically segregated, with two joined monoatomic clusters. Finally, at 40% Cu, we observe a CS morphology for small particles, while a JN-like structure is obtained for medium and big NPs. From our results, a CS to JN-like stability transition is observed as Cu is increased, this transition being slightly shifted to the left for big particles. This transition can be associated with the energy of Fe−Cu interactions that increases after a minimum value is reached (e.g., 30% Cu at big particles, see Table S1), which

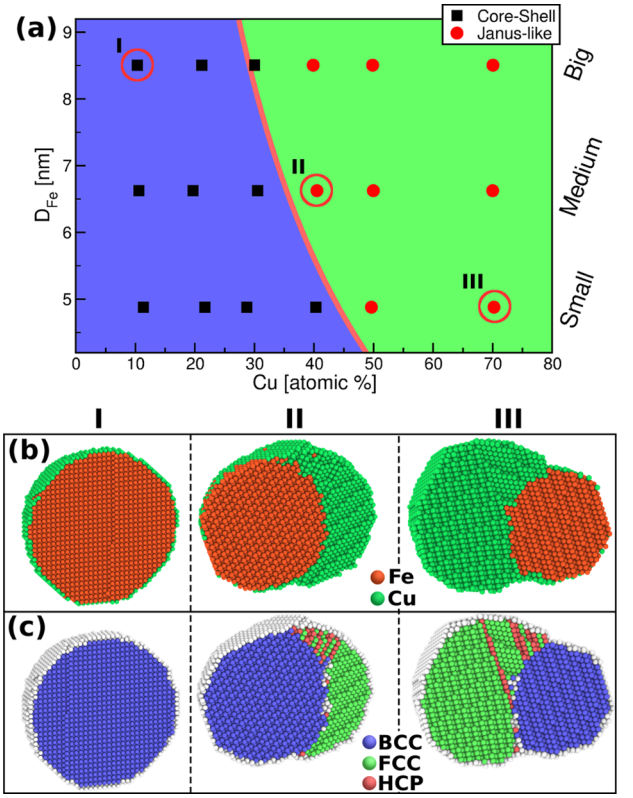

Figure 3. (a) Cluster structure as a function of size and Cu concentration. The pink line depicts the CS to JN-like stability transition from the continuous model. Cases I, II, and III are shown below. Cross-sectional views of FeCu particles encircled at (a), showing elemental composition (b), and structural defects (c). In (b), colors follow Figure 1, and in (c), atoms associated with the hcp phase (twins and stacking faults) are shown in red, whereas particles without any associated phase are shown in light gray.

DOI: 10.1021/acs.jpcc.7b11556
J. Phys. Chem. C XXXX, XXX, XXX−XXX

means that a segregated structure becomes preferred over CS morphologies as the Cu content gets higher.

Once we have determined the preferred morphology of the bimetallic particles at different Cu concentrations, the crystalline phases of the selected cases are reported. These phases are obtained from the common neighbor analysis (CNA) performed by the scientific visualization tool OVITO.[23] Figure 3c depicts the presence of mainly two crystalline phases: body-centered cubic (bcc, blue) and fcc (green) lattices, with light gray particles related to the atoms at the surface or defects. At 10% Cu, CNA shows only the bcc phase for all sizes. At 70% Cu, there are two phases: bcc phase for Fe and fcc for Cu. Finally, at 40% Cu, we can see that the NP shows mainly a bcc phase for Fe, while Cu is mainly ordered as an fcc lattice. Additionally, we can observe atoms associated with hexagonal closed-packed (hcp) structures (red) because of twins (single red planes) and stacking faults (SFs, double red planes) nucleated at the Fe−Cu interface.

To consider the coordination analysis of the optimized NPs, the radial distribution function (RDF), $g(r)$, is calculated and shown in Figure 4, for stable systems at 10, 40, and 70% Cu.

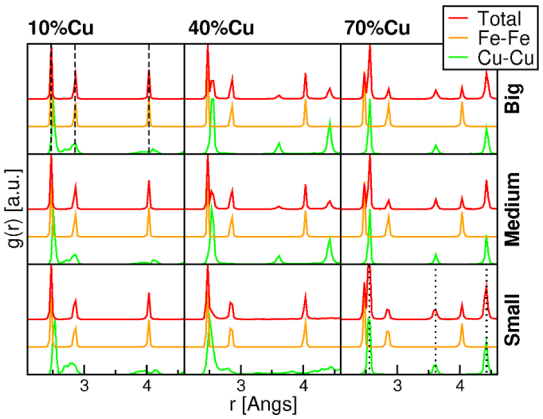

Figure 4. Total and partial RDF of FeCu particles as a function of the Cu concentration and size. Segmented and dotted lines correspond to three first peaks of the crystalline bcc and fcc lattices, respectively.

Here, we can see the coordination per element (brown and green lines for Fe and Cu, respectively) as well as the total RDF (red line) at different sizes. At the low Cu percentage, both Fe−Fe and the total RDF give the expected peaks of the bcc lattice (crystalline bcc peaks are depicted as segmented black lines), and even Cu−Cu shows a similar distribution of peaks. In contrast, at 70% Cu, the total $g(r)$ reflects the contribution of both bcc and fcc lattices associated with Fe−Fe and Cu−Cu, respectively (crystalline fcc peaks are depicted as dotted black lines). At 40% Cu, we have mixed results, where smaller NPs show mainly bcc lattice peaks, whereas medium and big NPs have the formation of both bcc and fcc phases. These results can be directly related to experimental diffraction results and lead us to expect a bcc phase of Fe at low Cu concentrations, while bcc and fcc phases are expected at high Cu concentrations.

3.3. Stress and Surface Energy. Figure 3c shows that minimized NPs exhibit structural defects in Cu. Because Cu has a low SF energy,[26] surface nucleation of SFs might be expected, as it has been reported for solid NPs[33] and nanowires.[34] Also, the accumulation of SFs leads to nanotwins.[35] These low-energy planar defects are not expected to contribute significantly to global structural transitions. A twin boundary is a sigma-type grain boundary, and Suzuki and Mishin have shown that interstitial diffusion across and along Sigma-type grain boundaries has lower activation energy than bulk diffusion.[36]

Figure 5 shows the final relaxed configuration, with dislocations and the surfaces of the Cu and Fe NPs, for the small case, and 50% Cu. There is one twin boundary, seen as a single plane of defective atoms, and two SFs, seen as double layers of atoms. Additionally, from Figure 5, it can be seen that the Cu atoms wrap around the outer surface of the roughly spherical Fe NP, leaving out only about half of the Fe surface and generating a Cu surface significantly larger than the initial Cu surface, and resulting in an enhanced Fe−Cu interaction. Additional information is given in Figure S1, showing the energy optimization and depicting some frames until the final configuration (F case in Figure S1a), while the mean square displacement shows a higher diffusion of Cu atoms. A similar behavior occurs for other cluster diameters and concentrations above the stability transition of CS and JN.

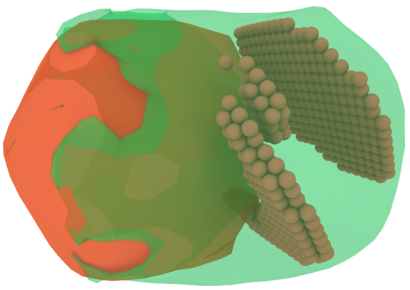

Figure 5. Defects for the small (5 nm Fe core) FeCu particle at 50% Cu after relaxation. SFs (double planes) and twin boundaries (single plane) are depicted with brown spheres. Cu envelops the red Fe cluster, leaving only a relatively small portion of uncovered Fe.

There are no important defects observed in Fe. This is as expected, given that the nucleation stress for dislocations is roughly proportional to the shear modulus of a given material,[37] and in Fe, the value is 116 GPa,[38] which is significantly larger than that in Cu (76 GPa).[26] For Fe nanowires, twins have been observed only for stress above 20 GPa,[39] which is much larger than that in the annealing process.

SF nucleation can occur from surface imperfections[40] but in our simulations is generally triggered from the Fe−Cu interface, where the stress concentration can occur during annealing. Nucleation leads to stress relaxation, and the interface is nearly stress-free, unlike what happens for semi-infinite planar interfaces.[41]

Planar defects can strengthen the NPs.[42] However, planar defects observed in our simulations are not stable and do not survive from one high temperature annealing cycle to another. SF recovery has been observed in nanocrystalline metals,[43] and detwinning can occur when surfaces are present.[44] Under room-temperature conditions, defects might survive and change mechanical and optical properties of the NPs.[1]

Miscibility can be modified by defects, as in ball milling of FeCu,[14] and this leads to a few Fe atoms going into the Cu cluster. These atoms migrate to the Cu surface or to the Fe−Cu interface.

3.4. Modeling the Energetic Stability of the FeCu Morphology. To study the structural stability of the FeCu NPs, we have developed a model based on the different energy

DOI: 10.1021/acs.jpcc.7b11556
J. Phys. Chem. C XXXX, XXX, XXX−XXX

atomic interactions for the two different cases: CS and JN-like structures, showing a structural map between these morphologies.

This model is based on the assumed immiscibility between Fe and Cu, a result also obtained from the optimization process, where an alloyed structure (mixed atoms) was found to be less energetically stable than our two main morphologies. This model considers a continuous representation for the NPs and assumes a spherical representation of the Fe cluster (see Figure 6), with Cu atoms then redistributed to produce a CS or segregated JN morphology, a condition based on the higher melting point of Fe compared to Cu, preserving the relevant features of the theoretical and experimental clusters.

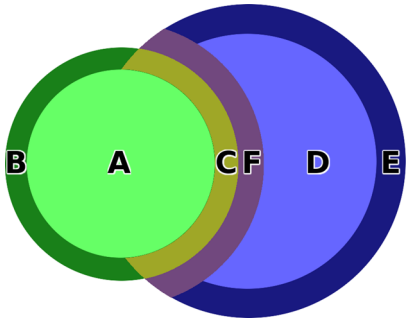

Figure 6. Schematic representation of the JN-like structure and the specific regions defined in the continuous model. Both Fe and Cu contributions are divided with (A,D) depicting bulk regions, (B,E) corresponding to free surfaces, and (C,F) related to interaction regions.

The total energy (per atom) is then determined by the contributions of the six regions in Figure 6; (A) iron bulk E^{Fe}_{bulk}, (B) iron surface E^{Fe}_{surf}, (C) iron interaction E^{Fe}_{int}, (D) copper bulk E^{Cu}_{bulk}, (E) copper surface E^{Cu}_{surf}, and (F) copper interaction E^{Cu}_{int} and defined as

$$E = X_A E^{Fe}_{bulk} + X_B E^{Fe}_{surf} + X_C E^{Fe}_{int} + X_D E^{Cu}_{bulk} + X_E E^{Cu}_{surf} + X_F E^{Cu}_{int} \quad (2)$$

where X_i corresponds to the number of atomic sites within each region, which depends on the NP volume and density. A more detailed explanation of each term of the continuous model is given in the Supporting Information. Figure 3a shows the structural map as a function of Cu % and particle size, finding both CS (light blue) and JN-like (green) regions as the most stable morphologies. The CS structure is found to be more stable at low Cu percentages and up to a condition associated with the formation of two Cu monolayers. At high Cu content, the energy of the bulk region becomes more important than Cu interaction energies, and therefore, a JN structure is preferred.

This model is parameterized by the energy contributions E^{Fe}_{bulk} = −4.12 eV/atom, E^{Fe}_{surf} = −3.55 eV/atom, E^{Fe}_{int} = −3.94 eV/atom, E^{Cu}_{bulk} = −3.53 eV/atom, E^{Cu}_{surf} = −3.06 eV/atom, and E^{Cu}_{int} = −3.51 eV/atom, which are obtained from the molecular dynamics simulations and are in agreement with the reported values for the cohesive energies.[45,46]

Additionally, Table 1 summarizes the total energy values of FeCu particles at different Cu percentages from the model, as well as the comparison with molecular dynamics simulations, finding a good agreement with a relative difference (Δr) less than 2%. The relative energy differences show that at high Cu percentages, where bulk Cu becomes more important, the model slightly underestimates the energy, with respect to the molecular dynamics simulations. At low Cu %, the model shows a small overestimation of the energy, where the Cu surface is one of the main contributions.

3.5. Experimental Evidence of FeCu Bimetallic NPs Morphology. To compare our simulations and model with experimental results, a synthesis of FeCu bimetallic NPs with two different proportions of Cu in the structure (10% Cu and 50% Cu) was performed using the simultaneous reduction chemical method and the experimental procedure reported by Wang and Zhang[47] and Xiao et al.,[48] obtaining a black material corresponding to bimetallic NPs. Figure 7 shows the scanning transmission electron microscopy (STEM) analysis and energy-dispersive X-ray spectroscopy (EDS) line profile of the particles in both nanomaterials. The profile for 10% Cu (Figure 7a) displays the presence of mainly Fe particles with low quantities of Cu around Fe, associated with the formation of oxide and CS structures. In contrast, for the case of 50% Cu, Figure 7b,c, displays two types of NPs, corresponding to separate Cu and Fe NPs, respectively. These results are consistent with the theoretical and modeling studies, finding that a low Cu proportion promotes a CS structure, while the increase of the "noble metal" concentration in bimetallic structures generates an evolution of the morphology of these particles, with the preference of segregated structures (JN-like) at 50% Cu, suggesting that there would be a critical number of Cu atoms before the stability transition from CS to other structures begins. This segregation has already been reported by Xiao et al., finding a separation of Fe and Cu after the synthesis of bimetallic NPs.[49]

Table 1. Total Energy of FeCu Particles as a Function of Cu Percentage from Molecular Dynamics and the Continuous Model within Their Relative Differences

E (eV/atom)		Cu %					
structures		10%	20%	30%	40%	50%	70%
big	simul	−3.99	−3.92	−3.87	−3.83	−3.76	−3.65
	model	−4.00	−3.91	−3.84	−3.79	−3.73	−3.63
	Δr %	0.32	−0.29	−0.80	−1.23	−0.72	−0.61
medium	simul	−3.96	−3.91	−3.85	−3.79	−3.74	−3.64
	model	−3.99	−3.91	−3.82	−3.75	−3.71	−3.61
	Δr %	0.67	0.05	−0.66	−1.01	−0.94	−0.79
small	simul	−3.92	−3.87	−3.83	−3.76	−3.72	−3.62
	model	−3.97	−3.88	−3.83	−3.73	−3.67	−3.58
	Δr %	1.22	0.30	−0.09	−0.99	−1.38	−1.13

DOI: 10.1021/acs.jpcc.7b11556
J. Phys. Chem. C XXXX, XXX, XXX−XXX

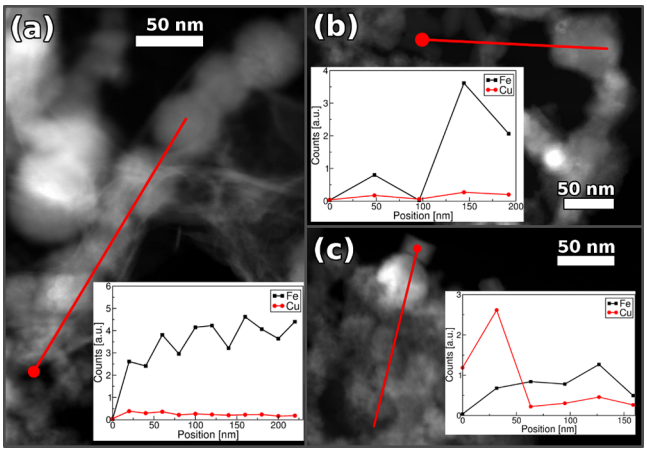

Figure 7. Linear mapping of the synthesized bimetallic NPs for (a) 10 and (b,c) 50% Cu, respectively. Initial position is defined with the red circle in the red line. (a) suggests a CS structure, while (b,c) suggest segregated or JN-like structures.

Additionally, we have added chemical analysis in the Supporting Information to support our results (see Figures S3 and S4), showing the scanning electron microscopy−EDS analysis performed on bimetallic material with 10% Cu (Figure S3a,b) and 50% Cu (Figure S4a,b), respectively. This quantitative characterization is consistent with STEM, and therefore, the presence of Fe and Cu in the bimetallic NPs was corroborated.

4. SUMMARY AND CONCLUSIONS

We studied the morphology of FeCu NPs by using a multistep optimization procedure, establishing Cu concentration conditions where CS or JN-like structures are the more energetically stable morphologies. At low Cu concentrations, Cu atoms wrap the Fe cluster following the Fe bcc lattice. Once we increase the Cu concentration, the shell of Cu atoms shows an fcc lattice until the stability transition point from CS to JN is reached. A segregated structure is obtained at high Cu content, with a bcc lattice for Fe and an fcc lattice for Cu. The Cu−Cu energy becomes more important as the Cu percentage is increased, while the Fe−Cu energy grows quickly until the first monolayer is built, and from there on forward, it has slow-paced growth as the Cu content increases. This effect leads to a stability transition point where it is more energetically expensive to surround the Fe core than to segregate the Cu atoms. This transition point is slightly shifted to a lower Cu concentration as the Fe nucleus size is increased. For large Cu content, twins and SFs were found, nucleated by the help of the Fe−Cu interface formed in JN-like structures. Although our multiple annealing cycles display convergence, the use of Monte Carlo simulations as in Erhart et al.[19] might display some features which cannot be observed within the relatively short simulation time scale. Nevertheless, we expect the CS to JN stability transition behavior to be observed for other materials and help to design bimetallic NPs at requested conditions, as a function of the elemental concentration. In this direction, future work might also consider other bimetallic NPs of technological interest,[6] as well as consider the incorporation of iron and copper oxide compounds. Finally, a continuous model for the immiscible FeCu system is proposed to obtain the most stable configuration, resulting in a structural map in agreement with the molecular dynamics simulations and experimental evidence. This model can be used for other NPs, provided the characteristic energies are calculated from atomistic simulations. The tailoring of certain structures for a given size and composition would also allow the possibility to engineer desired properties for technological applications.

■ ASSOCIATED CONTENT

Supporting Information

The Supporting Information is available free of charge on the ACS Publications website at DOI: 10.1021/acs.jpcc.7b11556.

Detailed description of the continuous model for JN-like and CS structures, obtaining the energy minimization of the system (PDF)

■ AUTHOR INFORMATION

Corresponding Author

*E-mail: samuel.baltazar@usach.cl, samuel.baltazar@gmail.com.

ORCID

Rafael I. Gonzalez: 0000-0003-2599-8404
Pamela Sepúlveda: 0000-0002-5221-4452
Nicolás Arancibia-Miranda: 0000-0002-0142-6922
Samuel E. Baltazar: 0000-0001-9826-9400

Author Contributions

The manuscript was written through contributions of all authors. All authors have given approval to the final version of the manuscript. The authors contributed equally.

Notes

The authors declare no competing financial interest.

■ ACKNOWLEDGMENTS

The authors thank the support of FONDECYT under grants 11100439 and 1161018, DICYT project 041631BR, the Basal Funding for Scientific and Technological Centers under project FB0807, NSF with project 1434897, scholarship grants CONICYT-PCHA "Doctorado Nacional" 2015-21150699 and CONICYT-PFCHA/Doctorado Nacional/2017-21170040. E.M.B. thanks funding from PICT2014-0696 and a SeCTyP grant. S.A. thanks the support of AFOSR Neuromorphics Inspired Science under grant FA9550-16-1-0384. This research was partially supported by the supercomputing infrastructure of the NLHPC (ECM-02) and partially supported by the supercomputing infrastructure of the HPC USACH-SEGIC (ECM-02).

■ REFERENCES

(1) Link, S.; Wang, Z. L.; El-Sayed, M. A. Alloy Formation of Gold-Silver Nanoparticles and the Dependence of the Plasmon Absorption on Their Composition. *J. Phys. Chem. B* **1999**, *103*, 3529−3533.
(2) Wu, M.-L.; Chen, D.-H.; Huang, T.-C. Synthesis of Au/Pd Bimetallic Nanoparticles in Reverse Micelles. *Langmuir* **2001**, *17*, 3877−3883.
(3) Agarwal, S.; Al-Abed, S. R.; Dionysiou, D. D. Enhanced Corrosion-Based Pd/Mg Bimetallic Systems for Dechlorination of Pcbs. *Environ. Sci. Technol.* **2007**, *41*, 3722−3727.
(4) Han, Y.; Yan, W. Bimetallic Nickel-Iron Nanoparticles for Groundwater Decontamination: Effect of Groundwater Constituents on Surface Deactivation. *Water Res.* **2014**, *66*, 149−159.
(5) Ma, C.; Chen, Y.; Chen, J. Surfactant-Assisted Preparation of Fecu Catalyst for Fischer-Tropsch Synthesis. *J. Braz. Chem. Soc.* **2015**, *26*, 1520−1526.
(6) Oviedo, O. A.; Leiva, E. P. M.; Mariscal, M. M. Thermodynamic Considerations and Computer Simulations on the Formation of

DOI: 10.1021/acs.jpcc.7b11556
J. Phys. Chem. C XXXX, XXX, XXX−XXX

Core−Shell Nanoparticles under Electrochemical Conditions. *Phys. Chem. Chem. Phys.* **2008**, *10*, 3561−3568.
(7) McNamara, K.; Tofail, S. A. M. Nanoparticles in Biomedical Applications. *Adv. Phys.: X* **2016**, *2*, 54−88.
(8) Andersin, J.; Honkala, K. First Principles Investigations of Pd-on-Au Nanostructures for Trichloroethene Catalytic Removal from Groundwater. *Phys. Chem. Chem. Phys.* **2011**, *13*, 1386−1394.
(9) Liu, W.-J.; Qian, T.-T.; Jiang, H. Bimetallic Fe Nanoparticles: Recent Advances in Synthesis and Application in Catalytic Elimination of Environmental Pollutants. *Chem. Eng. J.* **2014**, *236*, 448−463.
(10) Manning, B. A.; Hunt, M. L.; Amrhein, C.; Yarmoff, J. A. Arsenic(III) and Arsenic(V) Reactions with Zerovalent Iron Corrosion Products. *Environ. Sci. Technol.* **2002**, *36*, 5455−5461.
(11) Yan, W.; Herzing, A. A.; Li, X.-Q.; Kiely, C. J.; Zhang, W.-X. Structural Evolution of Pd-Doped Nanoscale Zero-Valent Iron (Nzvi) in Aqueous Media and Implications for Particle Aging and Reactivity. *Environ. Sci. Technol.* **2010**, *44*, 4288−4294.
(12) O'Carroll, D.; Sleep, B.; Krol, M.; Boparai, H.; Kocur, C. Nanoscalezero Valent Iron and Bimetallic Particles for Contaminated Site Remediation. *Adv. Water Resour.* **2013**, *51*, 104−122.
(13) Aslan, S.; Yalçin, K.; Hanay, Ö.; Yildiz, B. Removal of Tetracyclines from Aqueous Solution by Nanoscale Cu/Fe Bimetallic Particle. *Desalin. Water Treat.* **2015**, *57*, 14762−14773.
(14) Ma, E.; He, J.-H.; Schilling, P.-J. Mechanical Alloying of Immiscible Elements: Ag-Fe Contrasted with Cu-Fe. *Phys. Rev. B: Condens. Matter Mater. Phys.* **1997**, *55*, 5542−5545.
(15) Morales-Luckie, R. A.; Sanchez-Mendieta, V.; Arenas-Alatorre, J. A.; López-Castañares, R.; Perez-Mazariego, J. L.; Marquina-Fabrega, V.; Gómez, R. W. One-Step Aqueous Synthesis of Stoichiometric Fe−Cu Nanoalloy. *Mater. Lett.* **2008**, *62*, 4195−4197.
(16) Massalski, T. B. *Binary Alloy Phase Diagram*; ASM International, 1986.
(17) Taherkhani, F.; Seresht, P. F. Doping Effect on the Janus-Like Structure of a Copper−Iron Bimetallic Nanocluster and Its Solid−Liquid Phase Transition. *Prog. Theor. Exp. Phys.* **2015**, *2015*, 043I01.
(18) Akbarzadeh, H.; Mehrjouei, E.; Ramezanzadeh, S.; Izanloo, C. Ni-Co Bimetallic Nanoparticles with Core−Shell, Alloyed, and Janus Structures Explored by Md Simulation. *J. Mol. Liq.* **2017**, *248*, 1078−1095.
(19) Erhart, P.; Marian, J.; Sadigh, B. Thermodynamic and Mechanical Properties of Copper Precipitates in α-Iron from Atomistic Simulations. *Phys. Rev. B: Condens. Matter Mater. Phys.* **2013**, *88*, 024116.
(20) Mariscal, M. M.; Dassie, S. A.; Leiva, E. P. M. Collision as a Way of Forming Bimetallic Nanoclusters of Various Structures and Chemical Compositions. *J. Chem. Phys.* **2005**, *123*, 184505.
(21) Holec, D.; Zhou, L.; Riedl, H.; Koller, C. M.; Mayrhofer, P. H.; Friák, M.; Sob, M.; Körmann, F.; Neugebauer, J.; Music, D.; Hartmann, M.; Fischer, F. Atomistic Modeling-Based Design of Novel Materials. *Adv. Eng. Mater.* **2017**, *19*, 1600688.
(22) Plimpton, S. Fast Parallel Algorithms for Short-Range Molecular Dynamics. *J. Comput. Phys.* **1995**, *117*, 1−19.
(23) Stukowski, A. Visualization and Analysis of Atomistic Simulation Data with Ovito−the Open Visualization Tool. *Modell. Simul. Mater. Sci. Eng.* **2010**, *18*, 015012.
(24) Daw, M. S.; Baskes, M. I. Embedded-Atom Method: Derivation and Application to Impurities, Surfaces, and Other Defects in Metals. *Phys. Rev. B: Condens. Matter Mater. Phys.* **1984**, *29*, 6443−6453.
(25) Bonny, G.; Pasianot, R. C.; Castin, N.; Malerba, L. Ternary Fe−Cu−Ni Many-Body Potential to Model Reactor Pressure Vessel Steels: First Validation by Simulated Thermal Annealing. *Philos. Mag.* **2009**, *89*, 3531−3546.
(26) Mishin, Y.; Mehl, M. J.; Papaconstantopoulos, D. A.; Voter, A. F.; Kress, J. D. Structural Stability and Lattice Defects in Copper:Ab Initio, Tight-Binding, and Embedded-Atom Calculations. *Phys. Rev. B: Condens. Matter Mater. Phys.* **2001**, *63*, 224106.
(27) Bitzek, E.; Koskinen, P.; Gähler, F.; Moseler, M.; Gumbsch, P. Structural Relaxation Made Simple. *Phys. Rev. Lett.* **2006**, *97*, 170201.
(28) Nguyen, T. D.; Nguyen, C. C.; Tran, V. H. Molecular Dynamics Study of Microscopic Structures, Phase Transitions and Dynamic Crystallization in Ni Nanoparticles. *RSC Adv.* **2017**, *7*, 25406−25413.
(29) Shibuta, Y.; Watanabe, Y.; Suzuki, T. Growth and Melting of Nanoparticles in Liquid Iron: A Molecular Dynamics Study. *Chem. Phys. Lett.* **2009**, *475*, 264−268.
(30) Shibuta, Y.; Suzuki, T. Effect of Wettability on Phase Transition in Substrate-Supported Bcc-Metal Nanoparticles: A Molecular Dynamics Study. *Chem. Phys. Lett.* **2010**, *486*, 137−143.
(31) Shibuta, Y.; Suzuki, T. Melting and Solidification Point of Fcc-Metal Nanoparticles with Respect to Particle Size: A Molecular Dynamics Study. *Chem. Phys. Lett.* **2010**, *498*, 323−327.
(32) Lin, Z.; Leveugle, E.; Bringa, E. M.; Zhigilei, L. V. Molecular Dynamics Simulation of Laser Melting of Nanocrystalline Au. *J. Phys. Chem. C* **2010**, *114*, 5686−5699.
(33) Salah, S. B. H.; Gerard, C.; Pizzagalli, L. Influence of Surface Atomic Structure on the Mechanical Response of Aluminum Nanospheres under Compression. *Comput. Mater. Sci.* **2017**, *129*, 273−278.
(34) Weinberger, C. R.; Cai, W. Plasticity of Metal Nanowires. *J. Mater. Chem.* **2012**, *22*, 3277.
(35) Stukowski, A.; Albe, K.; Farkas, D. Nanotwinned Fcc Metals: Strengthening Versus Softening Mechanisms. *Phys. Rev. B: Condens. Matter Mater. Phys.* **2010**, *82*, 224103.
(36) Suzuki, A.; Mishin, Y. Atomistic Modeling of Point Defects and Diffusion in Copper Grain Boundaries. *Interface Sci.* **2003**, *11*, 131−148.
(37) Hirth, J. P.; Lothe, J. *Theory of Dislocations*; Krieger Publishing Company, 1992.
(38) Mendelev, M. I.; Han, S.; Srolovitz, D. J.; Ackland, G. J.; Sun, D. Y.; Asta, M. Development of New Interatomic Potentials Appropriate for Crystalline and Liquid Iron. *Philos. Mag.* **2003**, *83*, 3977−3994.
(39) Sainath, G.; Choudhary, B. K. Molecular Dynamics Simulations on Size Dependent Tensile Deformation Behaviour of [110] Oriented Body Centred Cubic Iron Nanowires. *Mater. Sci. Eng., A* **2015**, *640*, 98−105.
(40) Lu, Y.; Song, J.; Huang, J. Y.; Lou, J. Surface Dislocation Nucleation Mediated Deformation and Ultrahigh Strength in Sub-10-Nm Gold Nanowires. *Nano Res.* **2011**, *4*, 1261−1267.
(41) Kang, K.; Wang, J.; Beyerlein, I. J. Atomic Structure Variations of Mechanically Stable Fcc-Bcc Interfaces. *J. Appl. Phys.* **2012**, *111*, 053531.
(42) Lu, K.; Lu, L.; Suresh, S. Strengthening Materials by Engineering Coherent Internal Boundaries at the Nanoscale. *Science* **2009**, *324*, 349−352.
(43) Budrovic, Z.; Van Swygenhoven, H.; Derlet, P. M.; Van Petegem, S.; Schmitt, B. Plastic Deformation with Reversible Peak Broadening in Nanocrystalline Nickel. *Science* **2004**, *304*, 273−276.
(44) Lee, S.; Im, J.; Yoo, Y.; Bitzek, E.; Kiener, D.; Richter, G.; Kim, B.; Oh, S. H. Reversible Cyclic Deformation Mechanism of Gold Nanowires by Twinning−Detwinning Transition Evidenced from in Situ Tem. *Nat. Commun.* **2014**, *5*, 3033.
(45) Ludwig, M.; Farkas, D.; Pedraza, D.; Schmauder, S. Embedded Atom Potential for Fe−Cu Interactions and Simulations of Precipitate−Matrix Interfaces. *Modell. Simul. Mater. Sci. Eng.* **1998**, *6*, 19−28.
(46) Rose, J. H.; Smith, J. R.; Guinea, F.; Ferrante, J. Universal Features of the Equation of State of Metals. *Phys. Rev. B: Condens. Matter Mater. Phys.* **1984**, *29*, 2963−2969.
(47) Wang, C.-B.; Zhang, W.-X. Synthesizing Nanoscale Iron Particles for Rapid and Complete Dechlorination of Tce and Pcbs. *Environ. Sci. Technol.* **1997**, *31*, 2154−2156.
(48) Xiao, K.; Bao, Z.; Qi, X.; Wang, X.; Zhong, L.; Lin, M.; Fang, K.; Sun, Y. Unsupported Cufe Bimetallic Nanoparticles for Higher Alcohol Synthesis Via Syngas. *Catal. Commun.* **2013**, *40*, 154−157.
(49) Xiao, K.; Bao, Z.; Qi, X.; Wang, X.; Zhong, L.; Fang, K.; Lin, M.; Sun, Y. Structural Evolution of Cufe Bimetallic Nanoparticles for Higher Alcohol Synthesis. *J. Mol. Catal. A: Chem.* **2013**, *378*, 319−325.

DOI: 10.1021/acs.jpcc.7b11556
J. Phys. Chem. C XXXX, XXX, XXX−XXX